Journal of Dentistry 148 (2024) 105027

Contents lists available at ScienceDirect

Journal of Dentistry

journal homepage: www.elsevier.com/locate/jdent

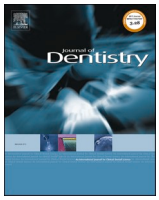

Tunable polymer-peptide hybrids for dentin tissue repair

Manuel Toledano [a], Enrique Fernández-Romero [a,b], Fátima S. Aguilera [a], Estrella Osorio [a,*], José A. Rodríguez-Santana [a], Macarena Garrido [a], Pedro A. Solís [a], Franklin García-Godoy [c], Raquel Osorio [a]

[a] University of Granada, Faculty of Dentistry. Colegio Máximo de Cartuja s/n, Granada 18071, Spain
[b] Medicina Clínica y Salud Pública PhD Programme, University of Granada, 18071 Granada, Spain
[c] Health Science Center, College of Dentistry, University of Tennessee, 875 Union Avenue, Memphis, TN 38103, United States

ARTICLE INFO

Keywords:
Dentin
Nanoparticles
Remineralization
Raman
Masson's trichrome staining
Tideglusib

ABSTRACT

Objectives: This study targets to assess the remineralization capability of conditioned dentin infiltrated with polymeric nanoparticles (NPs) doped with tideglusib (TDg) (TDg-NPs).
Methods: Dentin conditioned surfaces were infiltrated with NPs and TDg-NPs. Bonded interfaces were created, stored for 24 h and submitted to mechanical and thermal challenging. Resin-dentin interfaces were evaluated through nanohardness, Masson's trichrome staining microscopy, and Raman analysis.
Results: Dentin surfaces treated with TDg-NPs and load cycled produced higher nanohardness than the rest of the groups at the hybrid layer. At the bottom of the hybrid layer, all samples treated with TDg-NPs showed higher nanohardness than the rest of the groups. Active remineralization underneath the hybrid layer was detected in all groups after TDg application and load cycling, inducting new dentinal tubuli formation. After thermocycling, remineralization at the hybrid layer was not evidenced in the absence of NPs. Raman analysis showed increase mineralization, enriched carbonate apatite formation, and improved crosslinking and scaffolding of the collagen.
Conclusions: Mechanical loading on the specimens obtained after TDg-NPs dentin infiltration inducts an increase of mineralization at the resin/dentin interface, indicating remineralization of peritubular and intertubular dentin with augmented crystallographic maturity in crystals. Enriched collagen quality was produced, generating an adequate matrix organization to promote apatite nucleation, after tideglusib infiltration.
Clinical significance: At the present research, it has been proved the creation of reparative dentin, at the resin-dentin interface, after tideglusib dentin infiltration. Chemical stability, to favor integrity of the resin-dentin interface, is warranted in the presence of the TDg-NPs in the demineralized dentin collagen.

1. Introduction

Resin-composite restorations have usually exhibited a declined clinical effectiveness due to the challenges associated with the adhesive-resin–dentin bonds [1]. Adhesive dentistry aims to facilitate the complete infiltration of the resin across the entire thickness of the conditioned dentin, resulting in the formation of the hybrid layer (HL) [2,3]. Proteoglycans and Type I collagen fibrils are surrounded by a polymer chain, in this structure [3]. As a result of adhesive diffusion into demineralized dentin, a decreasing concentration gradient is formed, leaving collagen fibrils at the bottom of the HL (BHL) unprotected and vulnerable [4] (Fig. 1). However, dentin has demonstrated a considerable capacity for regeneration following damage [5].

Different mineral aggregate filling materials have been added into dental adhesives, in order to promote mineral deposition within the hybrid layer after an ion exchange [6]. Various resin fillers such as ceramic bioactive nanospheres made of hydroxyapatite (HAp), have also been suggested [7]. However, none of these materials offer an ptimal degradation kinetics and a sustained and controlled release [8]. The utilization of nanopolymeric particles (NPs) as calcium- and phosphate-sequestering materials have been presented as an alternative approach. These NPs are biocompatible and non-resorbable biomaterials, made of methacrylic acid, ethylene glycol dimethacrylate and 2-hydroxyethyl methacrylate, covalently connected [9,10]. Along the backbone of these polymeric NPs, there are chains of anionic carboxylate groups (i.e., COO-) that facilitate functionalization with metal cations or drugs containing amino groups [11].

* Corresponding author at: University of Granada, Faculty of Dentistry, Dental Materials Section, Colegio Máximo de Cartuja s/n, 18071 Granada, Spain.
E-mail address: meosorio@ugr.es (E. Osorio).

https://doi.org/10.1016/j.jdent.2024.105027
Received 13 February 2024; Received in revised form 23 April 2024; Accepted 25 April 2024
Available online 26 April 2024

Glossary

a.c.	arbitrary counts
AGE	advance glycation end products
β-cat	β-catenin
BHL	bottom of the hybrid layer
Bis-GMA	bisphenol A diglycidyl
DC	degree of conversion
EDX	energy dispersive X-ray
FWHM	full-width half-maximum
FTIR	Fourier-transform infrared spectroscopy
GMC	gradient in mineral content
GSK-3	glycogen-synthase-kinase 3
HAp	hydroxyapatite
HCA	hierarchical cluster analysis
HEMA	hydroxy ethyl methacrylate
Hi	nanohardness
HL	hybrid layer
KMC	K-means cluster
MMPs	matrix metalloproteinases
nano-DMA	nano-dynamic mechanical analysis
NPs	nanopolymeric particles
SB	single bond
SBFS	simulated body fluid solution
SiC	silicon carbide
TDg	tideglusib

Recently, Neves et al. (2017) [12] reported the performance of various small molecule GSK-3 antagonists which have been developed, in an effort to promote the natural processes of reparative dentin formation. Tideglusib (TDg), a small molecule GSK-3 inhibitor used in Alzheimer's disease treatment, has been proposed as a dentin repair agent [13]. Various methods for TDg delivery have been employed, such as a collagen sponge [12], or a hyaluronic acid-based hydrogel [5]. In the current research, hydrophilic polymeric nanostructured particles will serve as carriers to assess the in vitro clinical efficacy of TDg at the resin-dentin interface.

Exposure of demineralized unprotected collagen, either by resin or intrafibrillar mineral, may be subjected to degradation, mediated by endogenous matrix metalloproteinases (MMPs) in junction with their extracellular inhibitors. One in vitro method for testing consequences of aging involves challenging the resin-dentin interface with load cycling or testing the resistance of the resin-dentin interfaces when subjected to hydrolytic degradation under thermal stress. Load cycling and thermocycling of bonded specimens has been widely employed for in vitro assessment of resin-based dental materials [14].

The aim of this study was to evaluate the effect of the infiltration of polymeric nanoparticles doped with tideglusib into phosphoric acid-etched dentin before the adhesive application, in order to ascertain the ability to promote mineral deposition, to protect the hybrid layer, and to restore the original dentin mechanical properties at the decalcified hybrid layer. To evaluate mechanical recovery and remineralization at the hybrid layer, various techniques were used: Dentin mineral precipitation at the hybrid layer was indirectly assessed by evaluating nanohardness augmentation at the hybrid layer under various degradation methodologies and storage conditions [15]. By employing Masson's trichrome staining, we conducted a qualitative assessment of collagen encapsulation, observing color distinctions within the non-remineralized and remineralized interfacial areas. While the majority of research has concentrated on the mechanical features of the substrate, the microscopic or histological aspects of dentin, and the underlying molecular structure, essential for comprehending the impact of the disease on the mineral content and collagen matrix, has been scarcely investigated [16]. In this regard, Raman spectroscopy is a potent tool for directly obtaining data about the molecular composition of a specimen. Compared to traditional microscopic and histological techniques, Raman spectroscopy and cluster analysis are advantageous as they are fast, stain-free, non-intrusive and quantitative [17]. The null hypotheses to be tested are that TDg-NPs infiltration, into etched dentin, (1) does not affect nanomechanical properties at the resin-dentin interface and (2) does not enable mineral precipitation at the

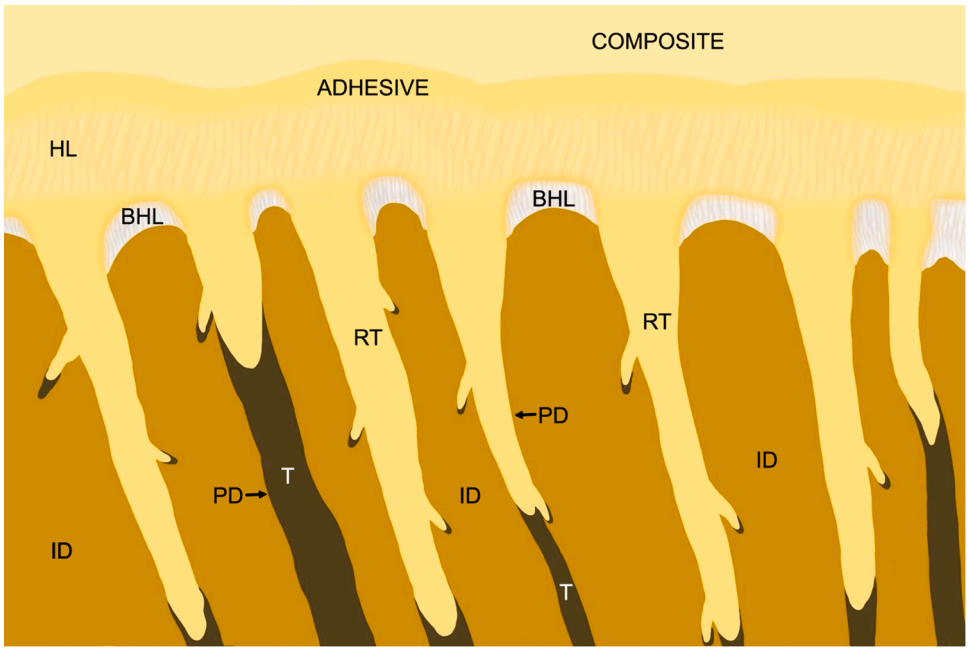

Fig. 1. Representative image, in scheme, of the resin-dentin interface. BHL, Bottom of the hybrid layer. Abbreviations: HL, Hybrid layer. ID, Intertubular dentin. PD, Peritubular dentin. T, Dentinal tubule. RT, Resin tag.

demineralized bonded interface.

2. Material and methods

2.1. Production of nanoparticles

The process of obtaining NPs applied the use of the polymerization precipitation method, which controlled the precipitation facilitated by a thermodynamic approach. Specifically, the Flory-Huggins model, based on Hansen's solubility parameters, was employed. This model centered on interactions among solvent molecules and the growth of polymer chains through hydrogen, polar bonding, and dispersion forces [18]. The backbone monomer for NPs design was 2-hydroxyethyl methacrylate, with methacrylic acid serving as the functional monomer, and ethylene glycol dimethacrylate employed as the cross-linker. Subsequently, half of the produced NPs were loaded with a peptide, tideglusib (Sigma-Aldrich, Chemie, Riedstr, Germany). The NPs loading process was conducted by immersion of 100 mg of NPs in 1 mL of 0.0017 mg/mL TDg solution for 2 h at room temperature under constant shaking (12 rpm) (rotator Orbit 300,445, JP Selecta, Barcelona, Spain). Then, the NPs were left until the solvent was completely evaporated, ensuring that all the TDg remains onto the NPs. Two types of NPs were obtained, undoped NPs and TDg-NPs.

2.2. Preparation of specimens for the bonding procedure, mechanical and thermal challenging

Thirty-six unerupted human third molars, preserved at 4 °C in a 0.5% chloramine T solution for no more than a month, were utilized for this study. Prior to their involvement, subjects provided informed consent, aligning with the Declaration of Helsinki and adhering to good clinical practice guidelines. The study received ethical approval from the Institutional Ethics Committee (1906/CEIH/2020).

The teeth were horizontally sectioned just below the dentin-enamel junction to expose sound dentin surfaces. These surfaces were then flatly polished to create a clinically relevant smear layer, utilizing 180-grit silicon carbide –SiC- abrasive paper. Subsequently, the dentin surfaces underwent etching (with 37% phosphoric acid, during 15 s), followed by rinsing and drying. Random allocation of experimental teeth ($n = 12$) to one of three groups was achieved through computer-generated randomization, facilitated by http://www.randomizer.org/form.htm. The allocation remained concealed in sealed envelopes until the time of bonding procedure. Just an ethanol solution was applied (30 s) (i), or an ethanol suspension of undoped-NPs (ii), and TDg-NPs (iii) (10 mg/mL) in each of the three experimental groups ($n = 12$), acting as primers. Ethanol was then evaporated for 30 s and, finally, Single Bond (SB) resin (3 M ESPE, St. Paul, MN, USA) was applied according to the manufacturer's instructions, to fulfill the conventional adhesive protocol. The sample preparation was conducted by one researcher, and a uniform adhesion protocol was implemented by a different researcher. For each tooth, a composite build-up (5 mm high) (Tetric EvoCeram, Ivoclar-Vivadent, Schaan, Liechtenstein) was performed using the incremental technique, in five 1 mm resin layers. The light-curing process was carried out with a Bluephase polywave light-emitting diode light-polymerizing unit (Bluephase G2, Ivoclar Vivadent AG, Schaan, Liechtenstein) at 1500 mW/cm^2 for 20 s. The output intensity was monitored with a curing radiometer (Model Bluephase meter, Ivoclar Vivadent AG, Schaan, Liechtenstein), ensuring a minimal output intensity of 1500 mW/cm^2 for all experiments. The restored teeth were stored in a dark environment and submerged in simulated body fluid solution (SBFS) for 24 h.

Three experimental groups were established, 1) control group, 2) undoped NPs and 3) TDg-NPs, with 12 specimens per group. The specimens were then divided into three sub-groups ($n = 4$) based on the challenging method: (1) Restored teeth stored in SBFS for 24 h, (2) load cycling with a sine wave form for 24 hs (259,200 cycles, 3 Hz) (S-MMT-250NB; Shimadzu, Tokyo, Japan) proceeding as in Sauro *et al.* 2009 [19], and (3) thermal cycling (100,000 cycles/ 5 °C and 55 °C) (SD Mechatronik, Germany) during approximately three months in distilled water [13]. Finally, the samples were sectioned into resin–dentin slabs and polished using ascending grit SiC abrasive papers (#1200 to #4000) on a water-cooled polishing device (Buehler-MetaDi, Buehler, Lake Bluff, IL, USA). The specimen preparation was concluded with a final ultrasonic cleaning (5 min) (Figure S1).

2.3. Nanoindentation testing

Dentin-resin slabs were submitted for nanoindentation testing. The nano-hardness was performed using a Hysitron Ti 950 nanoindenter (Hysitron, Minneapolis, MN). The nanoindenter was a Berkovich (three-sided pyramidal) diamond indenter tip (tip radius ~20 nm). It was calibrated against a fused quartz sample using a quasistatic force set-point of 5 μN. On each slab, three indentation lines 15(±5) μm from each other were made in different mesiodistal positions along the interface. Four indentation were performed in each straight line starting from the top of hybrid layer down to the underlying intertubular dentin in order to evaluate changes in the nanohardness (*Hi*) of the resin-dentin interface (Fig. 1). The apical-occlusal distance between each indentation was kept constant (5 ± 1 μm) by adjusting the distance intervals steps. Indentations were executed with a load of 4000 nN and a time function of 10 s. The procedure was performed in a hydrated condition by the application of a layer of ethylene glycol over the specimen surface, preventing water evaporation during a typical 25-to-30-min scanning period [20].

2.4. Masson's trichrome staining

Thirty-six resin–dentin bonded slices were used for the histomorphological evaluations. The medial aspects of each resin–dentin bonded slice were attached to a glass holder using a photocuring adhesive (Technovit 7210 VLC; Heraeus Kulzer, Werheim, Germany) and ground with SiC papers ranging from 800 to 4000 grits in a polisher (Apparatebau d-2000; Exakt Norderstedt, Germany) until reaching a thickness of approximately 10 μm. Masson's trichrome staining was applied to the slices in order to facilitate the differentiation of resin and non-resin encapsulation of the exposed collagen. This staining technique exhibits a high affinity for cationic elements of normally mineralized dentin type I collagen, resulting in green staining of collagen. In demineralized collagen, different colorations, generally red, appear. Collagen coated with adhesive stains orange, and pure adhesive appears beige. Subsequently, the stained sections on slides were dehydrated through ascending ethanol and xylene, cover-slipped, and examined under light microscopy (BH-2; Olympus, Tokyo, Japan) at $a \times 100$ magnification. One slice was prepared from each specimen, and the images were digitalized using a scanner (Agfa Twin 1200; Agfa-Gevaert NV, Mortsel, Belgium). Within each specimen, the presence or absence of a red band corresponding to demineralized dentin was observed. A qualitative assessment of collagen encapsulation was conducted by visualizing color differences within the interfacial zones of resin–dentin interfaces [17,21].

2.5. Raman spectroscopy and cluster analysis

A dispersive Raman spectrometer/microscope (Horiba Scientific Xplora, Villeneuve d'Ascq, France) was used to analyze dentin interfaces. A near-infrared diode laser spot size of ≈ 0.5μm^2, operating at 785 nm, was employed to measure the Raman signal (100 mW power at sample surface) from 400 to 1700 cm^{-1} Raman wavenumber. Chemical mappings of the interfaces were performed. For each specimen two areas 20 × 20 mm area of the interfaces at different sites were mapped using 1 mm spacing at X and Y axes, and each spectrum was measured by using 2 s acquisition time with 2 accumulations. For each mapping, using the

multivariate analysis tool (Isys, Horiba), a K-means cluster analysis (KMC) was performed, which includes a statistical pattern to generate independent clusters. The software to classify different natural groups of components used Hierarchical Cluster Analysis (HCA). The observed spectra were described at 400–1700 cm^{-1} with 10 complete overlapping Gaussian lines, suggesting homogeneous data for further calculations [22].

As the cluster centroids are essentially means of the cluster score for the elements of cluster, the mineral and organic components of the resin-dentin interface were examined for each cluster. A comparison of the spectra that were collected from the specimens which compose each subgroup might indicated complete overlap, suggesting similarity between both measurements. It was hence used for identifying significant spectral differences among distinct substrata. Clusters were created following Ward's technique and the dendrogram was calculated applying five factor spectra or principal components, corresponding with five different components at the resin-dentin interface (red, more mineralized dentin; green, dentin; blue, bottom of hybrid layer; purple, hybrid layer; yellow, adhesive). For each point of analysis, all spectra described for each cluster were averaged to obtain the mean cluster spectrum. At this point, the mineral (Table S1), organic components and degree of adhesive efficacy of dentin were calculated. a) The organic component of dentin was analyzed examining the following parameters:

Normalization: Phenyl group; the peak at 1003 cm^{-1}, which is assigned to C—C bond in the phenyl group, was used for normalization [23].

Crosslinking: AGEs (advance glycation end products)-pentosidine at 1550 cm^{-1}, interpreted as a marker of the aging process [24].

Nature and secondary structure of collagen: α-helices peak [1340 cm^{-1}]: This signal has been assigned to protein α-helices where intensity is sensitive to molecular orientation [22]. b) Degree of adhesive efficacy:

Degree of conversion of adhesive

Ratio 1637/1608. The peak appearing at 1637 cm^{-1} is associated with C = C of methacrylate, and the peak at 1608 cm^{-1} is related to C—C in phenyl of adhesive monomer [25].

Bis-GMA penetration

Ratio1113/1667. The peak appearing at 1113 cm^{-1} is associated with C—O-C of adhesive, and the peak at 1667 cm^{-1} is related to amide I [25,26].

Adhesive (Bis-GMA and HEMA) penetration

Ratio 1450/1667. The peak appearing at 1450 cm^{-1} is assigned to the CH_2 group of both Bis-GMA and HEMA, and the peak at 1667 cm^{-1} is related to amide I [25,26].

2.6. Statistical analysis

Mean nanohardness values were calculated in GPa and analyzed by analysis of variance including analysis of interactions ($p < 0.05$). NPs application and challenging method were independent factors. Student-Newman-Keuls ($p < 0.05$) was used for *post hoc* comparisons.

3. Results

3.1. Nanoindentation testing, nanohardness

Mean nanohardness (*Hi*) values (GPa) and Standard deviation (SD) attained at the different indentation zones in the experimental groups, are exposed in Fig. 2.

At the hybrid layer, samples treated with TDg-NPs after 24 h (0.55 GPa, SD 0.07) and mechanically loaded (0.49 GPa, SD 0.08) attained the highest nanohardness ($P < 0.05$). The control group after 24 h achieved the lowest *Hi* values (0.11 GPa, SD 0.03) ($P < 0.05$). The rest of the groups obtained intermediate values, without differences among them ($P > 0.05$), ranging from 0.35 GPa, SD 0.06 (dentin treated with TDg-NPs thermocycled) to 0.44 GPa, SD 0.10 (dentin treated with undoped NPs) (Fig. 2).

Any sample treated with TDg-NPs attained the highest *Hi* among all groups of study, at the bottom of the hybrid layer ($P < 0.05$), ranging from 0.62 GPa, SD 0.07 (dentin treated with TDg-NPs mechanically loaded) to 0.72 GPa, SD 0.12 (dentin treated with TDg-NPs after 24 h).

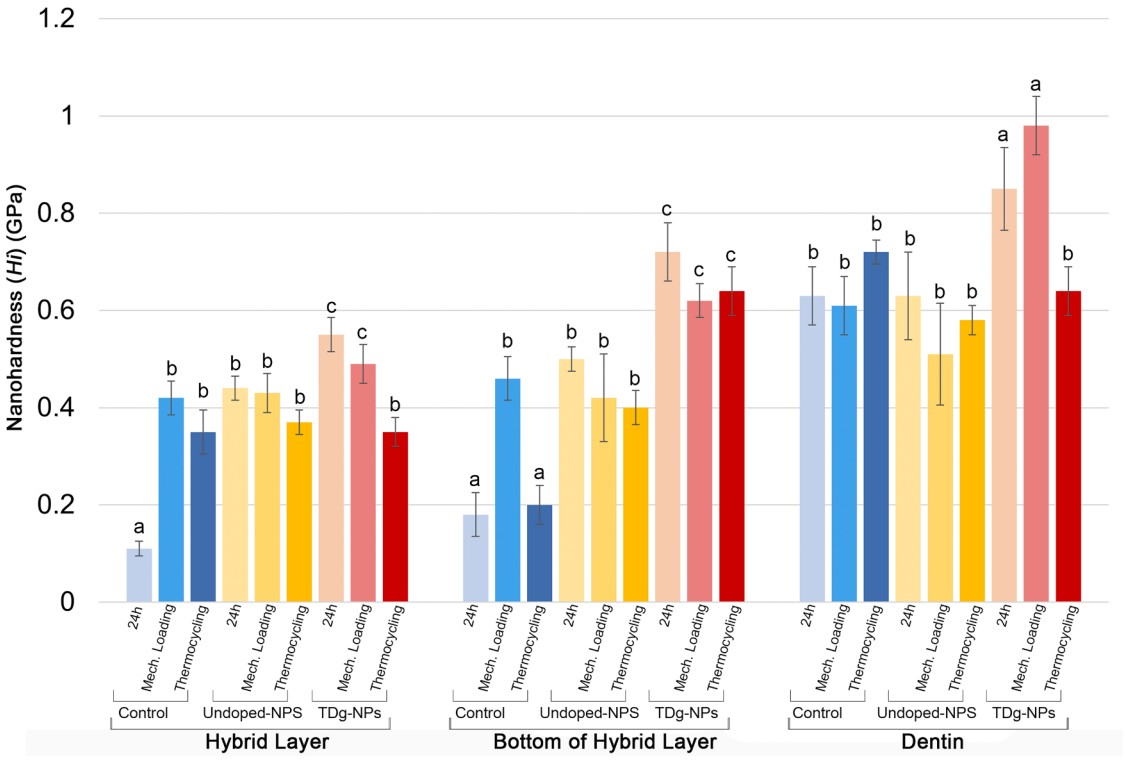

Fig. 2. Mean and standard deviation (SD) values of nanohardness (GPa) attained at the different experimental groups. Identical lowercase means no significant difference among distinct experimental groups at the same tested interface. Abbreviations: NPs, nanoparticles.

Specimens treated without NPs, except those mechanically loaded, achieved the lowest *Hi* values ($P < 0.05$) (0.18 GPa, SD 0.09 in the control group after 24 h; 0.20 GPa, SD 0.08 in the control group after thermocycling (Fig. 2).

At the intact dentin, those samples treated with TDg-NPs after 24 h (0.85 GPa, SD 0.17) and mechanically loaded (0.98 GPa, SD 0.12) showed the highest *Hi* among groups ($P < 0.05$) (Fig. 2).

3.2. Masson's trichrome staining

Representative images are shown in Fig. 3. An intense and wide red zone evidenced the existence of non-resin covered and demineralized dentin collagen in all groups, at 24 h of storage (Figs. 3A, 3B, 3C). Active remineralization at the base of the hybrid layer was detected in all groups after load cycling (Figs. 3D, 3E, 3F). Tubular dentin walls formation was detected, reproducing the sinusoidal primary curvatures (Fig. 3F). When specimens were thermocycled, remineralization at the hybrid layer was not evidenced in the absence of NPs (Fig. 3G) and in presence of undoped NPs (Fig. 3H). A faint and non-continuous red line was found at the hybrid layer that was formed after TDg-NPs dentin infiltration; green zones indicating intratubular and peritubular remineralization were observed within the resin-dentin interface (arrows), and some parts of the restoration showed total remineralization (Fig. 3I).

3.3. Raman spectroscopy and cluster analysis

3.3.1. Relative presence of minerals

Dentin treated with TDg-NPs showed higher phosphate peak intensities at both HL and BHL than dentin treated with undoped NPs, at 24 h of storage and after load cycling (Table 1). Thermocycling produced the maximum phosphate peak and area at the BHL of dentin samples treated with TDg-NPs, among groups (Table 1). The area of phosphate peak obtained the highest intensity at both the HL and BHL when TDg-NPs infiltrated the dentin at 24 h of storage and after load cycling, in comparison with the rest of the groups (control and undoped NPs). The carbonate peak intensity was highest at both the HL and BHL when TDg was used to infiltrate dentin after 24 h of storage and after load cycling. Thermocycling produced the highest carbonate intensity at the BHL when TDg was used for NPs doping. At 24 h of storage, the highest area of carbonate appeared when dentin was treated with TDg-NPs at both HL and BHL. When specimens were submitted to load cycling, those treated with TDg achieved the lowest carbonate area in comparison with the group of dentin treated with unloaded NPs. Thermocycling produced the lowest carbonate area among groups, at the HL of dentin treated with TDg, and produced the highest carbonate area at the BHL of dentin treated with TDg-NPs (Table 1).

3.3.2. Crystallinity

Crystallinity, at both HL and BHL, attained the lowest values when samples were treated with TDg-NPs and analyzed at 24 h of storage (Table 2). Between dentin groups infiltrated with NPs, those specimens load cycled and thermocycled and treated with TDg, attained the lowest crystallinity, referred to phosphate. In the case of carbonate, crystallinity at both HL and BHL attained the highest values when dentin was treated with TDg-NPs at specimens after 24 h of storage and load cycled. Those specimens achieved the lowest crystallinity when thermocycled (Table 2).

3.3.3. Gradient in mineral content (GMC)

GMC achieved the lowest value at both HL and BHL when samples were 24 h stored. When specimens were load cycled, at the HL, GMC obtained the lowest values when TDg-NPs was used to treat dentin. When specimens were thermocycled, dentin treated with TDg-NPs attained the highest GMC values at both HL and BHL (Table 2).

3.3.4. Crosslinking

When crosslinking was assessed, the HL of dentin treated with undoped NPs achieved the highest values among groups, and the BHL attained the highest intensity peak when dentin was infiltrated with TDg-NPs. Both HL and BHL in samples treated with TDg-NPs and submitted to load cycling and thermocycled showed the highest values among groups (Table 3).

3.3.5. Nature and secondary structure of collagen

Both HL and BHL of specimens load cycled showed the highest peak intensities after assessing Phenyl group. When nature and secondary structure of collagen were assessed, α-helices attained the highest peak intensities at both HL and BHL in interfaces created after TDg-NPs dentin infiltration in the groups of 24 h storage and thermocycled (Table 3).

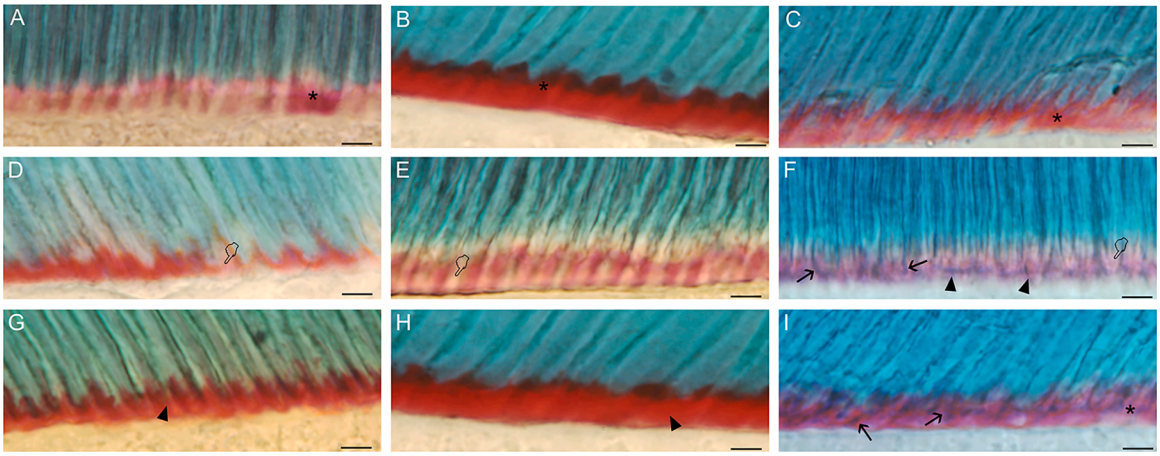

Fig. 3. Representative light micrographs of the interface specimens stained with Masson's trichrome. Mineralized dentin stained green/blue, adhesive stained beige, and exposed protein stained red. A-C Bonded resin–dentin interfaces, stained after 24 h of storage, without NPs, after undoped NPs, and TDg-NPs infiltration, respectively. A fringe of exposed collagen is observed at the hybrid layer in all groups (asterisks). d-F Bonded resin–dentin interfaces, stained after mechanical loading, in dentin treated without NPs, after undoped NPs, and TDg-NPs infiltration, respectively. The zone of exposed demineralized collagen was reduced. The intensity of the red color was diminished (pointers) and the intensity of the green/blue color raised at peritubular (arrows) and intertubular (arrow heads) dentin. G-I Bonded resin–dentin interfaces, stained after thermocycling, in dentin treated without NPs, after undoped NPs, and TDg-NPs infiltration, respectively. The demineralized collagen was not remineralized in absence of TDg, as the intensity of the red color was preserved (arrow heads). Clear signs of remineralization at the base of the hybrid layer was evidenced after TDg-NPs resin infiltration (arrows). *Scale bar* is 10 μm.

Table 1
Raman intensities and ratios of Relative Presence of Mineral components attained from experimental interfaces.

		Relative Presence of Mineral											
		Phosphate [961]						Carbonate [1070]					
		Peak			Area			Peak			Area		
		24 h	**LC**	**TC**	**24 h**	**LC**	**TC**	**24 h**	**LC**	**TC**	**24 h**	**LC**	**TC**
Control	HL	220.6	124.37	270.12	6291.19	4201.65	6988.84	44.14	33.24	48.78	6331.45	5289.68	6807.49
	BHL	306.54	337.24	282.8	8741.91	9452.03	7319.58	48.49	58.29	38.78	5824.48	3549.02	1874.94
	DEN 2	405.27	551.85	383.01	9857.57	14,020.80	9913.45	62.4	88.93	51.95	2763.46	3971.00	2300.53
	DEN 1	558.53	667.99	410.95	13,585.6	16,971.60	10,636.1	84.92	109.83	59.1	3760.75	4904.26	6404.52
Undoped-NPs	HL	164.16	94.56	207.24	4670.65	2745.32	6120.92	37.22	19.98	39.89	5135.48	3180.29	6028.51
	BHL	337.06	322.97	296.46	8175.92	9376.98	7513.23	56.46	49.79	42.31	3775.69	5609.18	5412.95
	DEN 2	459.52	501.76	417.65	11,146.30	12,999.70	10,584.4	77.86	75.10	56.41	4262.70	3659.21	2497.83
	DEN 1	577.39	708.54	569.82	14,005.20	17,600.10	14,441	88.93	103.45	76.49	4146.28	4619.31	3075.38
TDg-NPs	HL	198.87	393.14	115.33	6605.95	11,566.60	5286.88	44.74	63.05	33.19	6432.54	3064.6	5256.81
	BHL	377.40	526.37	327.61	10,957.30	15,486.40	9547.70	64.45	83.62	54.40	8268.00	4404.31	7567.83
	DEN 2	404.15	722.55	320.39	10,470.70	21,258.50	8285.10	61.00	115.94	46.50	2972.36	5163.43	2410.69
	DEN 1	578.43	776.55	521.26	14,444.10	19,591.10	13,002.80	87.10	121.83	75.32	3889.36	5425.84	3291.76

Abbreviations: NPs: nanoparticles; TDg: Tideglusib; HL: Hybrid layer; BHL: Bottom of hybrid layer; DEN: Dentin; 24 h: after 24 h of SBFS storage; LC: load cycling; TC: 100,000 thermal cycles. The peaks values had been normalized to the intensity of the Amide II band near 1510 cm^{-1}. Peaks positions are expressed in cm^{-1} and the intensity units are expressed in arbitrary counts (a.c.).

Table 2
Crystallinity and GMC ratio of mineral components attained from experimental interfaces.

		Crystallinity (FWHM)						GMC Ratio C/P		
		Phosphate $FWHM_P$			Carbonate $FWHM_C$					
		24 h	**LC**	**TC**	**24 h**	**LC**	**TC**	**24 h**	**LC**	**TC**
Control	HL	21.79	25.84	19.76	112.55	125.36	109.42	0.20	0.27	0.18
	BHL	21.79	21.41	19.76	93.73	46.84	37.10	0.16	0.17	0.14
	DEN 2	18.56	19.39	19.76	33.95	34.23	33.95	0.15	0.16	0.14
	DEN 1	18.56	19.39	19.76	33.95	34.23	84.32	0.15	0.16	0.14
Undoped-NPs	HL	21.73	22.18	19.76	108.11	125.36	109.42	0.23	0.21	0.18
	BHL	18.51	22.18	19.76	51.52	87.74	37.10	0.17	0.15	0.14
	DEN 2	18.51	19.78	19.76	42.07	37.39	33.95	0.17	0.15	0.14
	DEN 1	18.51	18.96	19.76	35.76	34.23	84.32	0.15	0.15	0.14
TDg-NPs	HL	25.40	22.48	35.16	112.84	37.30	124.73	0.22	0.16	0.29
	BHL	22.18	22.48	22.27	100.30	40.45	109.05	0.17	0.16	0.17
	DEN 2	19.78	22.48	19.74	37.39	34.14	39.81	0.15	0.16	0.15
	DEN 1	19.06	19.25	19.04	34.23	34.14	33.50	0.15	0.16	0.14

Abbreviations: NPs: nanoparticles; TDg: Tideglusib; HL: Hybrid layer; BHL: Bottom of hybrid layer; DEN: Dentin; FWHM: Full-width half-maximum; GMC: Gradient in mineral content (ratio 1070/961); 24 h: after 24 h of SBFS storage; LC: load cycling; TC: 100,000 thermal cycles. The peaks values had been normalized to the intensity of the Amide II band near 1510 cm^{-1}. Peaks positions are expressed in cm-1 and the intensity units are expressed in arbitrary counts (a.c.).

Table 3
Raman intensities and ratios of organics components attained from experimental interfaces (crosslinking and nature of collagen).

		Crosslinking			Nature and secondary structure of collagen					
		AGEs-Pentosidine [1550]			Phenyl (norm.) [1003]			α-helices [1340]		
		24 h	**LC**	**TC**	**24 h**	**LC**	**TC**	**24 h**	**LC**	**TC**
Control	HL	2.13	4.83	0.82	47.2	40.26	45.05	15.52	23.59	19.50
	BHL	1.26	4.58	1.10	32.27	43.97	24.18	10.61	16.78	10.37
	DEN 2	1.32	5.53	0.5	38.65	56.70	30.23	9.68	19.46	12.48
	DEN 1	1.85	5.20	0.88	49.00	69.21	42.44	11.35	16.89	16.42
Undoped-NPs	HL	4.45	7.55	2.03	35.15	24.59	40.64	22.48	18.71	13.77
	BHL	3.25	1.18	2.23	39.77	40.61	35.51	16.00	14.74	9.70
	DEN 2	2.02	1.99	1.48	62.37	53.92	36.83	14.43	13.76	7.49
	DEN 1	2.44	1.57	1.98	52.48	62.95	48.15	11.05	17.26	8.85
TDg-NPs	HL	3.25	8.91	2.67	42.20	40.89	41.71	31.03	17.24	25.43
	BHL	4.45	8.24	2.45	54.31	53.57	41.43	24.43	19.04	21.38
	DEN 2	2.02	8.63	1.22	37.96	69.83	25.92	16.59	19.58	15.35
	DEN 1	2.44	9.15	0.96	56.18	66.97	40.15	15.67	23.56	18.21

Abbreviations: NPs: nanoparticles; TDg: Tideglusib; HL: Hybrid layer; BHL: Bottom of hybrid layer; A: amide; AGEs: advanced glycation end products; norm: Normalization. 24 h: after 24 h of SBFS storage; LC: load cycling; TC: 100,000 thermal cycles. For the organics components the peaks values had been normalized to the intensity of the Amide II band near 1510 cm^{-1}. Peaks positions are expressed in cm^{-1}, and the intensity units are expressed in arbitrary counts (a.c.).

3.3.6. Adhesive

The highest degree of conversion of the adhesive (DC) at both HL and BHL, at 24 h of storage, was attained when specimens were infiltrated with undoped NPs. When samples were load cycled, HL and BHL of dentin infiltrated with TDg-NPs achieved the highest DC of the infiltrated resin adhesive, among groups. Among thermocycled specimens, the BHL of the interfaces promoted with TDg-NPs achieved the highest DC of the infiltrated resin. The highest Bis-GMA and adhesive penetrations at both HL and BHL were obtained in the samples after 24 h storage and in the thermocycled specimens (Table 4).

The corresponding HCA Raman images (clusters) and results (centroids) are reflected at the Figs. 4 and 5, respectively. The chemical compounds and the spatial distribution of the main spectra were revealed by HCA results and exhibited five different clustered groups in contiguous traces of the scatter plots (Fig. 5). Two clusters were analyzed in the present research (Fig. 4), the hybrid layer and the bottom of the hybrid layer. Hybrid layer of samples treated with TDg-NPs and mechanically loaded showed the highest phosphate peak among groups when HCA were analyzed (Fig. 4F). Figs. 4C, 4F and 4I exposed higher existence of phosphate at the bottom of the hybrid layer than in the rest of the groups when NPs were doped with TDg, regardless the type of challenging. The analysis of variances only made to correspond a 21 % of the total mapping to the bottom of the hybrid layer (Figs. 4F, 5F, blue area), in comparison to control group (Figs. 4D, 5D) when specimens were load cycled. This trend was similarly followed after thermocycling (Figs. 4G, 5G blue area, 4I, 5I blue area). The hybrid layer of specimens treated with TDg-NPs and thermocycled reflected the highest variance (27 %) (Fig. 4I, purple area) and the lowest phosphate peak (115.33 a.c. -arbitrary counts-) (Table 1) intensity (Fig. 6I, red area), among groups. Dentin samples treated with TDg-NPs, after load cycling, attained the highest phosphate peak intensity among groups (Fig. 6F).

4. Discussion

At a whole, resin dentin interfaces treated with TDg-NPs showed the highest nanomechanical performance, in terms of nanohardness (*Hi*), at both HL and BHL among groups (Fig. 2). Therefore, the first null hypothesis to be tested must be rejected. Mineral precipitation at the HL, BHL and even at intact dentin, may have contributed to this improved nanomechanical performance [27,28] of the TDg-NPs doped resin-dentin bonded interfaces [13]. At the clinical scenarios, nanocrystalline hydroxyapatite is segregated into extrafibrillar and intrafibrillar mineral components. Hence, the rise in *Hi* of the partially demineralized and infiltrated collagen is properly associated with minerals deposits at the resin-dentin interface [29], particularly within the intrafibrillar section [30,31]. Thus, tideglusib appeared to promote mineral deposits onto the demineralized dentin facilitating functional mineralization, allowing mineral precipitation within the demineralized collagen. This was observed as a reduction in the red color intensity at the resin-dentin interface (Fig. 3C), indicating a relative advancement of the remineralization front. As a result, certain non-uniform and discontinuous zones beneath the adhesive layer display fewer pink and red areas (Fig. 3C). At the Masson's trichrome staining, this was indicative of a greater mineral precipitation into the demineralized collagen [15]. The existence of peptides at the interface could have generated electrostatic attraction for soluble ions, leading to a localized increase in supersaturation zones. This phenomenon may have facilitated mineral nucleation [32].

Mechanical loading significantly increased *Hi* at both HL and BHL, after using TDg-NPs (Fig. 2). According to the Masson's trichrome staining results, there are evidences of remineralization at the resin-dentin interface in all experimental groups submitted to mechanical loading, regardless the presence or not of NPs (Figs. 2, 3D, 3E, 3F). Mineralized dentin, appearing as new green/blue stained peritubular and intertubular dentin, is remarkable, especially when TDg-NPs were infiltrated, which showed an almost absence of unprotected collagen layer. Additionally, a development of new dentinal tubuli crossing the demineralized collagen was noted, signifying the remineralization of both peritubular and intertubular dentin. (Fig. 3F). Specific peptides are preferentially absorbed onto peritubular dentin, precisely in the locations where they predominantly exert their remineralizing functions [33]. The new precipitated occurred not only at the HL but at the first 5–20 μm of the tubule lengths [34,35]. On the other hand, undoped NPs dentin infiltration revealed a clear presence of unprotected decalcified dentin at the interface, allowing to observe the poor mineral gain at the partially-demineralized dentin layer (Figs. 3B, 3E, 3H). Moreover, mechanical loading has been observed to enhance the resistance of collagen against enzymatic degradation of unprotected [36].

A remineralized collagen fringe, in samples treated with TDg-NPs, was adverted covering the tubular walls and even at intertubular dentin (Fig. 3I) in comparison with both control group (Fig. 3G) and samples treated with undoped-NPs (Fig. 3H) when specimens were thermocycled. Masson's trichrome staining observations established a limited red zone, indicating decalcified and resin uncovered dentin in all specimens submitted to thermocycling (Figs. 3G, 3H), except when TDg-NPs (Fig. 3I) were used for resin-dentin infiltration. The observed outcome can be attributed to the limited remineralization capacity within the intrafibrillar section [30], *i.e.*, it is simply a precipitation of mineral [37] in interfaces without TDg (Fig. 2). Furthermore, the more pronounced reddish coloration was a consequence of the lower degree of Bis-GMA [1113/A-1], adhesive penetration [1453/1667] and degree of conversion of the adhesive that attained these two groups, *i.e.*, control and undoped NPs (Table 4). Even more, after using TDg-NPs, any signs of demineralized and/or exposed protein (red stain) were detectable in

Table 4
Raman intensities ratios of adhesive components attained from experimental interfaces after proposal challenges.

		Adhesive											
		1113			DC [1637/1608]			Bis-GMA Penetration [1113/A-I]			Adhesive Penetration [1453/1667]		
		24 h	**LC**	**TC**	**24 h**	**LC**	**TC**	**24 h**	**LC**	**TC**	**24 h**	**LC**	**TC**
Control	ADH	55.69	50.02	65.67	0.70	0.40	0.48	3.31	5.95	4.42	5.39	6.60	6.45
	HL	47.56	52.95	47.98	0.74	0.53	0.74	2.78	2.87	2.70	4.43	4.21	4.11
	BHL	27.95	29.97	15.41	0.78	0.69	0.90	2.56	1.99	1.77	3.66	2.81	2.44
Undoped-NPs	ADH	45.77	103.71	60.59	1.03	0.62	0.59	1.88	164.62	4.05	3.42	117.71	6.05
	HL	29.27	38.55	48.05	0.94	0.69	0.63	1.70	3.42	3.30	2.78	5.19	4.93
	BHL	22.09	27.37	33.05	1.17	1.10	0.72	1.46	1.69	2.66	2.10	2.73	3.92
TDg-NPs	ADH	14.64	49.83	102.38	0.26	0.66	0.43	9.76	2.91	26.05	10.65	4.30	27.97
	HL	45.00	23.96	62.26	0.80	0.89	0.83	2.95	1.55	2.82	5.38	1.77	5.12
	BHL	43.87	31.57	45.36	1.00	1.09	0.89	2.26	1.62	2.26	3.65	1.96	4.22

Abbreviations: NPs: nanoparticles; TDg: Tideglusib; ADH: Adhesive; HL: Hybrid layer; BHL: Bottom of hybrid layer; DEN: Dentin; DC: Degree of conversion of adhesive; Bis-GMA: bisphenol A diglycidyl methacrylate; A-I: Amide I; 24 h: after 24 h of SBFS storage; LC: load cycling; TC: 100,000 thermal cycles. The peaks values had been normalized to the intensity of the Amide II band near 1510 cm^{-1}. Peaks positions are expressed in cm^{-1} and the intensity units are expressed in arbitrary counts (a.c.).

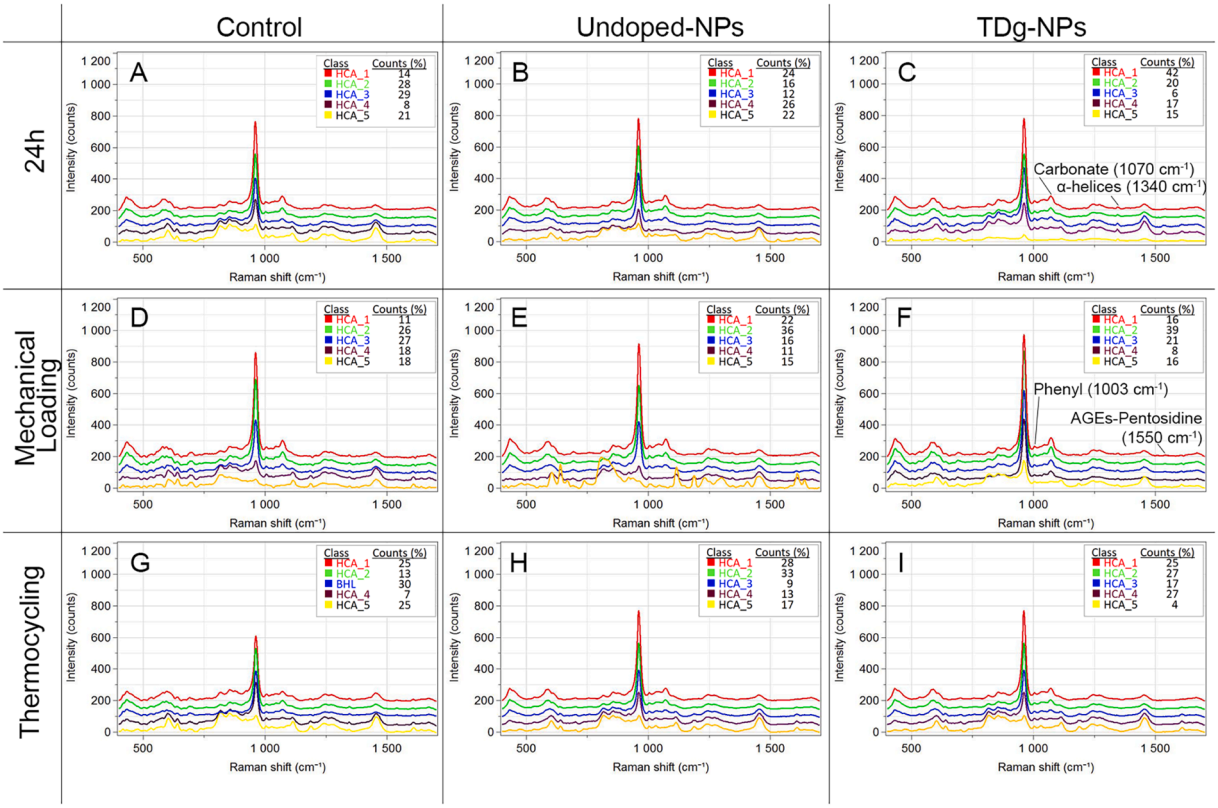

Fig. 4. Spectra from hierarchical cluster analysis (HCA) results (centroids) of the dentin interfaces analyzed at 24 h of storage: control group (A), treated with undoped-NPs (B) and tideglusib-doped NPs (C). Images from same groups when submitted to mechanical loading (D, E, F, respectively) and to thermocycling (G, H, I, respectively). HL, hybrid layer; BHL, bottom of hybrid layer.

some parts of the restoration (Fig. 3I). Thus, porosity may have diminished after applying TDg-NPs, as both red color intensity and width were clearly reduced. After thermocycling, synthesis and alkaline phosphatase activity and stimulations of proteins have been demonstrated in vivo and in vitro [13,38], and after using in vitro prebiotic peptides [39]. As a consequence, a more protected HL and BHL was shown along the whole resin-dentin interface when using TDg-NPs at the interface (Fig. 3I).

The Raman analysis further confirmed these findings. Dentin interfaces treated with TDg-NPs exhibited the highest mineralization observed, as evidenced by the peak (Fig. 4C) and area values of both phosphate (PO_4) (961 cm^{-1}) and carbonate (CO_3^{2-}) (1070 cm^{-1}) bands, particularly when NPs were doped with tideglusib (Table 1). Therefore, the second null hypothesis must also be rejected. Tetrahedral PO_4 group (P-O bond) within hydroxyapatite is characterized by the Raman phosphate peak at 961 cm^{-1}. Monitoring the intensity of this peak has been used to assess the potential increase in phosphate content [40], reflecting the augmentation in phosphate peak intensities when the 2D micro-Raman analysis was performed (Figs. 6C, 6F). In the present study, similar trend was followed by the CO_3^{2-} group, indicating the formation of new mineral in the previous partially demineralized dentin regions. These indexes complied with the highest relative degree of mineralization [41,42] (Table 1). The higher relative presence of minerals affected, at the whole resin-dentin interface but, specifically at the BHL that unveiled the maximum intensity peaks not only at 24 h of storage, but at all challenging groups (load cycling and thermocycling) (Table 1). This meant major presence of calcium phosphate precipitates at the resin-dentin interface, that was appreciated even when samples became treated with TDg-NPs and stored for 24 h (Fig. 3C) and after measuring the intensity of the phosphate peak (Fig. 6A). The referred interface showed exposed collagen but with a patent mineralization front at the base of the HL, reducing its wideness. A strong remineralization fringe was noticed at the BHL when samples treated with TDg were load cycled (Fig. 3F) or thermocycled (Fig. 3I). The remineralization front was more discontinuous in thermocycled samples than in load cycled specimens treated with TDg-NPs, but mechanical loading facilitated more advanced intratubular and peritubular mineralization (Fig. 3F).

A single-point spectroscopy approach proves insufficient for accurately characterizing the biochemical composition of the dentin substrate. Instead, the incorporation of bi-dimensional (2D) data analysis techniques with spatial information is crucial [43,44]. Our 2D-micro-Raman analysis, as confirmed by HCA results and cluster analysis, revealed the spatial distribution of main spectra and chemical compounds. HCA demonstrated five distinguishable clustered groups in adjacent traces of the scatter plots, in function of similar conditions of featuring [45], with each cluster represented by a different color [46]. At the interface of specimens treated with TDg-NPs, the corresponding HCA Raman results (centroids) obtained when specimens were subjected to load cycling demonstrated a general increase in the phosphate peak (Fig. 4F), in comparison with the samples treated with unloaded NPs (Fig. 4E), indicating mineral gain. This phosphate peak augmentation was clearly represented at the 2D micro-Raman map of 961 cm^{-1} intensities, where the redder area was visibly greater in mechanically loaded samples treated with TDg-NPs (Fig. 6F). The centroid corresponding to the hybrid layer (HCA_4) (Figure 5F/purple area), purple plot in Fig. 4F, slightly decreased the area of the hybrid layer (from 11 to 8 intensity counts) after load cycling of samples treated with TDg-NPs in comparison with unloaded NPs. The mineral gain that occurred at the demineralized collagen made to decrease the percentage of variance at dentin treated with TDg-NPs. This trend was reverted at the bottom of the hybrid layer (HCA_3), where variances changed from 11% in samples infiltrated with unloaded NPs until 21% when specimens infiltrated with TDg-NPs were mechanically loaded. These outcomes need further

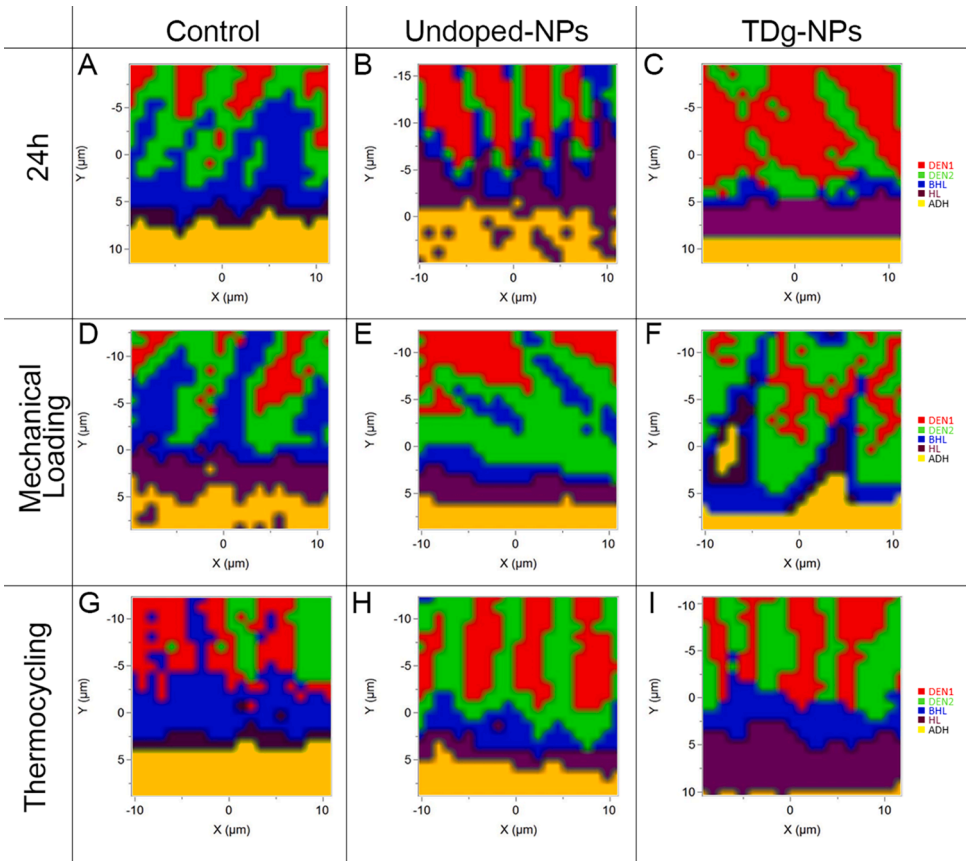

Fig. 5. Raman analysis [K-means clustering (KMC) map of the Raman profile] of the dentin interfaces analyzed at 24 h of storage: control interfaces (A), treated with undoped NPs (B) and tideglusib-doped NPs (C). Images from the same groups when submitted to mechanical loading (D, E, F, respectively) and thermocycling (G, H, I, respectively). Three levels of HCA clustering are shown. Areas of distinct colors have differences in Raman spectral distribution and chemical composition. Each cluster is assigned to a different color (red and green, dentin; purple, hybrid layer; blue, bottom of hybrid layer; yellow, adhesive), thus obtaining a false color-image of the substrate on the basis of similar spectral features. At the 2D micro-Raman, blue represents the lowest peak intensity, while the red represents the highest. DEN1 and DEN2, dentin 1 and dentin 2; HL, hybrid layer; BHL, bottom of hybrid layer; ADH, adhesive.

research in future investigations.

The formed hybrid layers when specimens were treated with TDg-NPs and submitted to thermocycling increased their percentages of variances (27%) (Fig. 4I) and the purple area (cluster in Fig. 5I), in comparison with the control group (7 %) (Fig. 4G), and with the group where unloaded NPs were used (Figs. 4H) (13%) (clusters in Figs. 5G, 5H, respectively). It is speculated that the augmented area of the hybrid layer that may be perceived at the Fig. 5I may be associated to an increase of extrafibrillar mineral, considering that this group did not increase its values of nanohardness after thermal cycling (40) (Fig. 2). The opposite occurred when HCA regarding the bottom of the hybrid layer was analyzed, that ranged from 30% of variance in the control group (Fig. 4G), until 9% in specimens treated with unloaded NPs (Fig. 4H). This reduction makes sense, as a gain of minerals at the demineralized collagen web is linked to a reduction in unprotected collagen [30]. Peaks at 1340 cm^{-1} associated with α-helices were also heightened in samples treated with tideglusib (Fig. 4), indicating increased sensitivity to molecular orientation aimed at facilitating further crystallization [22] (Table 3). The gradient in mineral content (GMC) at the hybrid layer of interfaces promoted by TDg-NPs thermocycled achieved the highest values among groups (0.29), but the lowest values of nanohardness (Fig. 2). This relative increase in mineral at HL was of amorphous nature, but crystalline at the BHL, where lower values of GMC were obtained, with high *Hi* values. The highest GMC that was obtained at the BHL at interfaces created after TDg-NPs infiltration at 24 h (0.17) (Table 2) correlates with the maximum *Hi* value (0.64 GPa) obtained when compared with both control and undoped NPs groups (Fig. 2). Hence, a much thinner unprotected demineralized collagen layer than those seen for both control and undoped NPs groups were observed (Fig. 3C). GMC, as result, meaning lower carbonate substitution for phosphate, pointing out higher maturity and crystallinity in comparison with the control group, related to a decline of amorphous calcium phosphate compounds [41,42].

Crystallinity, in general showed an amorphization process in all groups of study after infiltrating dentin with TDg-NPs (Table 2), as the full-width half-maximum (FWHM) increased at both HL and BHL, except when carbonate was assessed in the load cycled specimens (Table 2). Carbonated apatite is a precursor of hydroxyapatite [22], as it is unstable. Biological apatite is calcium deficient and contains substantial amounts of carbonate. The observed increase in the carbonate peak (1070 cm^{-1}) in samples treated with TDg-NPs (Table 1), indicates a higher presence of carbonate apatite in these samples when compared with the rest of the groups. This amorphization is likely associated with the incorporation of carbonate as a substituent for PO_4^3 in the apatite lattice [22]. Alterations in the phosphate band and peak in response to the existence of carbonate in the lattice or changes in the spectral region related to carbonate content can be manifested as the growth of a carbonate peak [47]. FWHM shows a broad increase in crystallographic maturity, or crystallinity, in minerals at the interface [42] (Table 2). This was numerically evidenced at Table 2 and graphically at Figs. 4C and 4F. Thereupon, the hybrid layer at mechanically loaded interfaces obtained after TDg-NPs infiltrated dentin have shown the lowest peak values (22.48) (crystallinity) and, by contrast, the bottom of the hybrid layer obtained the highest values (22.48) (amorphization). Amorphous

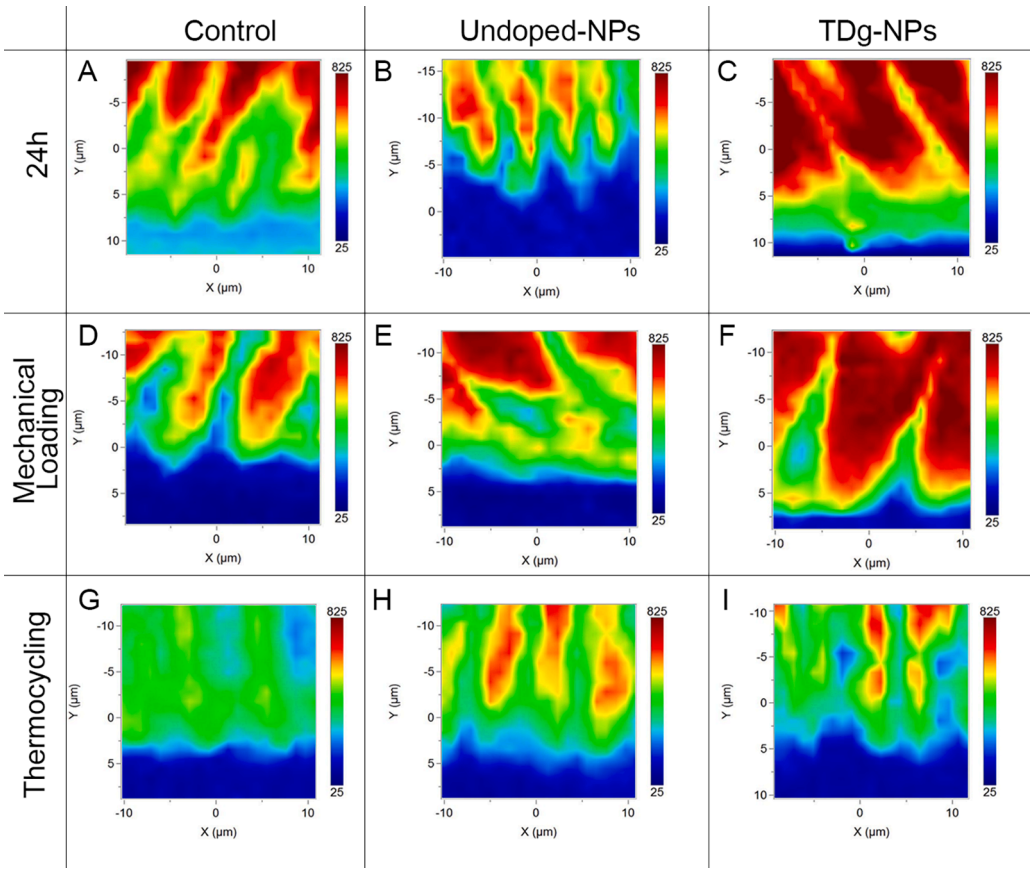

Fig. 6. Raman analysis [2D micro-Raman map of 961 cm^{-1} intensities] of the dentin interfaces analyzed at 24 h of storage: control (A), treated with undoped NPs (B) and tideglusib-doped NPs (C). Interfaces from the same groups when submitted to mechanical loading (D, E, F, respectively) and thermocycling (G, H, I, respectively). At the 2D micro-Raman, blue represents the lowest peak intensity, while the red represents the highest.

calcium phosphate establishes a localized environment rich in ions, providing favorable conditions for the in situ formation of prenucleation clusters. Consequently, this process facilitates further remineralization of dentin [48]. On the contrary, if crystalline calcium phosphates are formed, they will have long degradation times, requiring months or even years to release ions for remineralization [49].

The increase in mineral content was concurrently linked to the maximum crosslinking of collagen in samples treated with TDg-NPs (Table 3). Typically, an elevation in collagen crosslinking takes place following mineral precipitation [50,51], that may be considered to be the base for the enhancement of mechanical performance of dentin (Fig. 2) [52]. In general, resin-dentin interfaces infiltrated with TDg-NPs submitted to load cycling attained the highest peak of AGEs-pentosidine, at 1550 cm^{-1} (Table 3). After the application of tideglusib, mechanical loading could have triggered the conversion of keto-amines (immature cross-links), resulting in a more pronounced and sharper peak with a noticeable shift at 1550 cm^{-1}, at both HL and BHL. Pentosidine, identified as the primary component of advanced glycation end products (AGE) [53], strongly indicates ribose or ribonucleotide metabolites as potential precursors [24]. The high relative intensity peak corresponding to the AGES-pentosidine, at 1550 cm^{-1}, is generally associated with the formation of non-reducible crosslinks, suggesting that the initial remineralization process is intrafibrillar. Consequently, collagen can be viewed as an active scaffold promoting the formation of oriented crystalline hydroxyapatite within the fibrils [54,55].

Improvements in the nature and secondary structure of collagen were exhibited across the resin-dentin interface, following the infiltration of dentin with TDg-NPs, as the peak intensity of the phenyl group (1003 cm^{-1}) reached the highest values when the peptide was nano-carried into the demineralized collagen (Table 3). In contrast, specimens not treated with tideglusib displayed poor collagen matrix quality, characterized by a lack of conformation and organization [56, 57]. Mechanical stimuli applied to dentin infiltrated with TDg-NPs improved the nature and secondary structure of collagen throughout the entire resin-dentin interface compared to dentin infiltrated with other biomaterials (Table 3). Prior to the appearance of hydroxyapatite crystals, an increase in the protein-dependent spectral signal at phenylalanine was observed [22].

The present research provides evidence of the therapeutic activity of the experimental TDg-NPs, representing, to the best of our knowledge, the only available results from combined methodologies, including nano-indentation, Raman spectroscopy, and Masson's trichrome staining, to analyze TDg-NPs resin-dentin interfaces subjected to mechanical loading and thermocycling.

These outcomes have sufficiently provided information on biophysic-chemical structure of dentin treated with peptides-NPs carried-drugs for essential clinical applications. Reparative dentin formation at the resin-dentin interface has been demonstrated after tideglusib dentin infiltration. Among other factors, remineralization can occur through modifications in mechanical properties, (nanoindentation) [58–60], changes in mineral composition (X-ray diffraction, EDX, or FTIR spectroscopy analysis) [34,58], and changes in histomorphological and microstructural appearance evaluated through microradiography, µCT, AFM, scanning probe microscopy, scanning electron microscopy or dye-assisted optical or confocal microscopy [58,59]. While there is usually some correlation between these analyses, they are complementary, and the study acknowledges certain limitations, emphasizing the need for further research. The interpretation of low-resolution stained images may introduce uncertainty regarding the significance of observed differences in mineral apposition at the resin-dentin interface

among the tested groups. It highlights the necessity for transmission electron microscopy associated with diffraction analysis for accurate assessment of intrafibrillar collagen remineralization at the hybrid layer.

5. Conclusion

The application of mechanical loading to specimens subjected to TDg-NPs dentin infiltration induces an increase in mineralization at the resin/dentin interface. Dentin surfaces conditioned and infiltrated with TDg-NPs doped adhesive promote remineralization of peritubular and intertubular dentin. Following load cycling, this group forms minerals characterized by Raman bands indicative of an enriched carbonated apatite with enhanced crystallographic maturity at the interface. Despite an overall increase in mineral presence and phosphate and carbonate peak intensities after load cycling, the interface experiences diminished crystallinity and a gradient of mineral content. Collagen crosslinking ratios shift towards higher frequencies after load cycling, particularly in the presence of tideglusib at the interface, highlighting collagen's favorable nature for scaffolding and subsequent mineralization.

Dentin surfaces treated with TDg-NPs, resin-infiltrated, and subjected to load cycling exhibit elevated nanomechanical properties. Consequently, thinner unprotected collagen layers are observed compared to control and undoped NPs groups. Moreover, many samples show no signs of demineralization at the bottom of the resin-dentin inter-diffusion zone. The associated mineral precipitation is linked to an increase in the relative presence of minerals. Furthermore, the organic components enable the observation of an enriched collagen matrix quality, generating an organized matrix to facilitate apatite nucleation.

CRediT authorship contribution statement

Manuel Toledano: Writing – review & editing, Writing – original draft, Visualization, Validation, Supervision, Project administration, Methodology, Investigation, Funding acquisition, Formal analysis, Conceptualization. **Enrique Fernández-Romero:** Writing – review & editing, Visualization, Methodology, Data curation. **Fátima S. Aguilera:** Writing – review & editing, Writing – original draft, Visualization, Methodology, Investigation, Data curation. **Estrella Osorio:** Writing – review & editing, Writing – original draft, Visualization, Software, Resources, Methodology, Investigation, Data curation. **José A. Rodríguez-Santana:** Writing – review & editing, Investigation. **Macarena Garrido:** Writing – review & editing, Investigation. **Pedro A. Solís:** Writing – review & editing, Investigation. **Franklin García-Godoy:** Writing – review & editing, Writing – original draft, Visualization, Resources, Investigation, Data curation. **Raquel Osorio:** Writing – review & editing, Writing – original draft, Visualization, Supervision, Project administration, Methodology, Investigation, Funding acquisition, Formal analysis, Conceptualization.

Declaration of competing interest

The authors declare that they have no known competing financial interests or personal relationships that could have appeared to influence the work reported in this paper.

Acknowledgements

The present study was supported by Grant PID2020–114694RB-I00 funded by MCIN/AEI 10.13039/501100011033. This research is part of E. F-R.'s Ph.D. research study.

Supplementary materials

Supplementary material associated with this article can be found, in the online version, at doi:10.1016/j.jdent.2024.105027.

References

[1] J. Kim, R.M. Vaughn, L. Gu, R.A. Rockman, D.D. Arola, T.E. Schafer, K.K. Choi, D. H. Pashley, F.R. Tay, Imperfect hybrid layers created by an aggressive one-step self-etch adhesive in primary dentin are amendable to biomimetic remineralization in vitro, J. Biomed. Mater. Res. A 93A (2010) 1225–1234, https://doi.org/10.1002/jbm.a.32612.

[2] J. De Munck, P.E. Van den Steen, A. Mine, K.L. Van Landuyt, A. Poitevin, G. Opdenakker, B. Van Meerbeek, Inhibition of Enzymatic Degradation of Adhesive-Dentin Interfaces, J. Dent. Res. 88 (2009) 1101–1106, https://doi.org/10.1177/0022034509346952.

[3] L. Breschi, A. Mazzoni, F. Nato, M. Carrilho, E. Visintini, L. Tjäderhane, A. Ruggeri, F.R. Tay, E.D.S. Dorigo, D.H. Pashley, Chlorhexidine stabilizes the adhesive interface: a 2-year in vitro study, Dent. Mater. 26 (2010) 320–325, https://doi.org/10.1016/j.dental.2009.11.153.

[4] D.H. Pashley, F.R. Tay, L. Breschi, L. Tjäderhane, R.M. Carvalho, M. Carrilho, A. Tezvergil-Mutluay, State of the art etch-and-rinse adhesives, Dent. Mater. 27 (2011) 1–16, https://doi.org/10.1016/j.dental.2010.10.016.

[5] A. Alaohali, C. Salzlechner, L.K. Zaugg, F. Suzano, A. Martinez, E. Gentleman, P. T. Sharpe, GSK3 Inhibitor-Induced Dentinogenesis Using a Hydrogel, J. Dent. Res. 101 (2022) 46–53, https://doi.org/10.1177/00220345211020652.

[6] R. Osorio, M. Yamauti, S. Sauro, T.F. Watson, M. Toledano, Experimental resin cements containing bioactive fillers reduce matrix metalloproteinase-mediated dentin collagen degradation, J. Endod. 38 (2012) 1227–1232, https://doi.org/10.1016/j.joen.2012.05.011.

[7] A. Besinis, R. van Noort, N. Martin, Remineralization potential of fully demineralized dentin infiltrated with silica and hydroxyapatite nanoparticles, Dent. Mater. 30 (2014) 249–262, https://doi.org/10.1016/j.dental.2013.11.014.

[8] C. Wu, Y. Zhang, W. Fan, X. Ke, X. Hu, Y. Zhou, Y. Xiao, $CaSiO_3$ microstructure modulating the in vitro and in vivo bioactivity of poly(lactide-co-glycolide) microspheres, J. Biomed. Mater. Res. A 98 (2011) 122–131, https://doi.org/10.1002/jbm.a.33092.

[9] A.L. Medina-Castillo, J.F. Fernandez-Sanchez, A. Segura-Carretero, A. Fernandez-Gutierrez, Micrometer and Submicrometer Particles Prepared by Precipitation Polymerization: Thermodynamic Model and Experimental Evidence of the Relation between Flory's Parameter and Particle Size, Macromolecules 43 (2010) 5804–5813, https://doi.org/10.1021/ma100841c.

[10] R. Osorio, C.A. Alfonso-Rodríguez, A.L. Medina-Castillo, M. Alaminos, M. Toledano, Bioactive Polymeric Nanoparticles for Periodontal Therapy, PLOS ONE 11 (2016) e0166217, https://doi.org/10.1371/journal.pone.0166217.

[11] M.T. Osorio, R. Toledano, H. Huang, M. Toledano-Osorio, R. Osorio, C.Y.C. Huang, F. García-Godoy, Effect of doxycycline doped nanoparticles on osteogenic/cementogenic and anti-inflammatory responses of human cells derived from the periodontal ligament, J. Dent. 137 (2023), https://doi.org/10.1016/j.jdent.2023.104668.

[12] V.C.M. Neves, R. Babb, D. Chandrasekaran, P.T. Sharpe, Promotion of natural tooth repair by small molecule GSK3 antagonists, Sci. Rep. 7 (2017) 39654, https://doi.org/10.1038/srep39654.

[13] M. Toledano, F.S. Aguilera, E. Fernández-Romero, A.J.S. Lagos, M. Bonilla, C. D. Lynch, R. Osorio, Dentin remineralization using a stimuli-responsive engineered small molecule GSK3 antagonists-functionalized adhesive, Dent. Mater. (2023), https://doi.org/10.1016/j.dental.2023.12.010.

[14] F. Monticelli, R. Osorio, M. Toledano, F.R. Tay, M. Ferrari, In vitro hydrolytic degradation of composite quartz fiber-post bonds created by hydrophilic silane couplings, Oper. Dent. 31 (2006) 728–733, https://doi.org/10.2341/05-151.

[15] R. Osorio, I. Cabello, A.L. Medina-Castillo, E. Osorio, M. Toledano, Zinc-modified nanopolymers improve the quality of resin-dentin bonded interfaces, Clin. Oral Investig. 20 (2016) 2411–2420, https://doi.org/10.1007/s00784-016-1738-y.

[16] Y. Liu, X. Yao, Y.W. Liu, Y. Wang, A Fourier transform infrared spectroscopy analysis of carious dentin from transparent zone to normal zone, Caries Res 48 (2014) 320–329, https://doi.org/10.1159/000356868.

[17] M. Toledano, F.S. Aguilera, E. Osorio, I. Cabello, M. Toledano-Osorio, R. Osorio, Self-etching zinc-doped adhesives improve the potential of caries-affected dentin to be functionally remineralized, Biointerphases 10 (2015) 031002, https://doi.org/10.1116/1.4926442.

[18] A.L. Medina-Castillo, Thermodynamic principles of precipitation polymerization and role of fractal nanostructures in the particle size control, Macromolecules 53 (2020) 5687–5700, https://doi.org/10.1021/acs.macromol.0c00973.

[19] S. Sauro, F. Mannocci, M. Toledano, R. Osorio, D.H. Pashley, T.F. Watson, EDTA or H3PO4/NaOCl dentine treatments may increase hybrid layers' resistance to degradation: a microtensile bond strength and confocal-micropermeability study, J. Dent. 37 (2009) 279–288, https://doi.org/10.1016/j.jdent.2008.12.002.

[20] A.G. Schwartz, J.D. Pasteris, G.M. Genin, T.L. Daulton, Stavros Thomopoulos, Mineral distributions at the developing tendon enthesis, PloS One 7 (2012) e48630, https://doi.org/10.1371/journal.pone.0048630.

[21] M. Toledano, F.S. Aguilera, E. Osorio, I. Cabello, R. Osorio, Microanalysis of thermal-induced changes at the resin-dentin interface, Microsc. Microanal. 20 (2014) 1218–1233, https://doi.org/10.1017/S1431927614000944.

[22] C. Wang, Y. Wang, N.T. Huffman, C. Cui, X. Yao, S. Midura, R.J. Midura, J. P. Gorski, Confocal Laser Raman Microspectroscopy of Biomineralization Foci in UMR 106 Osteoblastic Cultures Reveals Temporally Synchronized Protein Changes Preceding and Accompanying Mineral Crystal Deposition, J. Biol. Chem. 284 (2009) 7100–7113, https://doi.org/10.1074/jbc.M805898200.

[23] C. Xu, Y. Wang, Cross-linked demineralized dentin maintains its mechanical stability when challenged by bacterial collagenase, J. Biomed. Mater. Res. B Appl. Biomater. 96 (2011) 242–248, https://doi.org/10.1002/jbm.b.31759.

[24] D.R. Sell, V.M. Monnier, Structure elucidation of a senescence cross-link from human extracellular matrix: implication of pentoses in the aging process, J. Biol. Chem. 264 (1989) 21597–21602, https://doi.org/10.1016/S0021-9258(20)88225-8.
[25] C. Xu, Y. Wang, Collagen cross-linking increases its biodegradation resistance in wet dentin bonding, J. Adhes. Dent. 14 (2012) 11–18, https://doi.org/10.3290/j.jad.a21494.
[26] Y. Wang, P. Spencer, Hybridization efficiency of the adhesive/dentin interface with wet bonding, J. Dent. Res. 82 (2003) 141–145, https://doi.org/10.1177/154405910308200213.
[27] A.A. Dawasaz, R.A. Togoo, Z. Mahmood, A. Azlina, K.Thirumulu Ponnuraj, Effectiveness of self-assembling peptide (P11-4) in dental hard tissue conditions: a comprehensive review, Polymers 14 (2022) 792, https://doi.org/10.3390/polym14040792.
[28] A.C. Profeta, F. Mannocci, R. Foxton, T.F. Watson, V.P. Feitosa, B. De Carlo, R. Mongiorgi, G. Valdré, S. Sauro, Experimental etch-and-rinse adhesives doped with bioactive calcium silicate-based micro-fillers to generate therapeutic resin–dentin interfaces, Dent. Mater. 29 (2013) 729–741, https://doi.org/10.1016/j.dental.2013.04.001.
[29] Y. Li, T.T. Thula, S. Jee, S.L. Perkins, C. Aparicio, E.P. Douglas, L.B. Gower, Biomimetic mineralization of woven bone-like nanocomposites: role of collagen cross-links, Biomacromolecules 13 (2012) 49–59, https://doi.org/10.1021/bm201070g.
[30] M. Balooch, S. Habelitz, J.H. Kinney, S.J. Marshall, G.W. Marshall, Mechanical properties of mineralized collagen fibrils as influenced by demineralization, J. Struct. Biol. 162 (2008) 404–410, https://doi.org/10.1016/j.jsb.2008.02.010.
[31] L.E. Bertassoni, S. Habelitz, J.H. Kinney, S.J. Marshall, G.W. Marshall Jr., Biomechanical Perspective on the Remineralization of Dentin, Caries Res 43 (2009) 70–77, https://doi.org/10.1159/000201593.
[32] M. Gungormus, F. Tulumbaci, Peptide-assisted pre-bonding remineralization of dentin to improve bonding, J. Mech. Behav. Biomed. Mater. 113 (2021) 104119, https://doi.org/10.1016/j.jmbbm.2020.104119.
[33] D.G. Moussa, J.A. Kirihara, Z. Ye, N.G. Fischer, J. Khot, B.A. Witthuhn, C. Aparicio, Dentin priming with amphipathic antimicrobial peptides, J. Dent. Res. 98 (2019) 1112–1121, https://doi.org/10.1177/0022034519863772.
[34] A.C. Profeta, F. Mannocci, R. Foxton, T.F. Watson, V.P. Feitosa, B. De Carlo, R. Mongiorgi, G. Valdré, S. Sauro, Experimental etch-and-rinse adhesives doped with bioactive calcium silicate-based micro-fillers to generate therapeutic resin-dentin interfaces, Dent. Mater. 29 (2013) 729–741, https://doi.org/10.1016/j.dental.2013.04.001.
[35] M. Toledano, I. Cabello, F.S. Aguilera, E. Osorio, M. Toledano-Osorio, R. Osorio, Improved sealing and remineralization at the resin-dentin interface after phosphoric acid etching and load cycling, Microsc. Microanal. 21 (2015) 1530–1548, https://doi.org/10.1017/S1431927615015317.
[36] M. Toledano, E. Osorio, F.S. Aguilera, S. Sauro, I. Cabello, R. Osorio, In vitro mechanical stimulation promoted remineralization at the resin/dentin interface, J. Mech. Behav. Biomed. Mater. 30 (2014) 61–74, https://doi.org/10.1016/j.jmbbm.2013.10.018.
[37] Y. Xu, J. Wu, H. Wang, H. Li, N. Di, L. Song, S. Li, D. Li, Y. Xiang, W. Liu, X. Mo, Q. Zhou, Fabrication of electrospun poly(L-lactide-co-ε-caprolactone)/collagen nanoyarn network as a novel, three-dimensional, macroporous, aligned scaffold for tendon tissue engineering, Tissue Eng. Part C Methods 19 (2013) 925–936, https://doi.org/10.1089/ten.TEC.2012.0328.
[38] E. Lozupone, C. Palumbo, A. Favia, M. Ferretti, S. Palazzini, F.P. Cantatore, Intermittent compressive load stimulates osteogenesis and improves osteocyte viability in bones cultured “in vitro, Clin. Rheumatol. 15 (1996) 563–572, https://doi.org/10.1007/BF02238545.
[39] J.A. Cowan, Influence of the weak nuclear force on metal-promoted autocatalytic strecker synthesis of amino acids: formation of a chiral pool of precursors for prebiotic peptide and protein synthesis, Life Basel Switz 14 (2023) 66, https://doi.org/10.3390/life14010066.
[40] H. Milly, F. Festy, T.F. Watson, I. Thompson, A. Banerjee, Enamel white spot lesions can remineralise using bio-active glass and polyacrylic acid-modified bio-active glass powders, J. Dent. 42 (2014) 158–166, https://doi.org/10.1016/j.jdent.2013.11.012.
[41] K. Karan, X. Yao, C. Xu, Y. Wang, Chemical profile of the dentin substrate in non-carious cervical lesions, Dent. Mater. 25 (2009) 1205–1212, https://doi.org/10.1016/j.dental.2009.04.006.
[42] A.G. Schwartz, J.D. Pasteris, G.M. Genin, T.L. Daulton, S. Thomopoulos, Mineral distributions at the developing tendon enthesis, PLOS ONE 7 (2012) e48630, https://doi.org/10.1371/journal.pone.0048630.
[43] C. Krafft, G. Steiner, C. Beleites, R. Salzer, Disease recognition by infrared and Raman spectroscopy, J. Biophotonics 2 (2009) 13–28, https://doi.org/10.1002/jbio.200810024.
[44] J.A. Timlin, A. Carden, M.D. Morris, R.M. Rajachar, D.H. Kohn, Raman spectroscopic imaging markers for fatigue-related microdamage in bovine bone, Anal. Chem. 72 (2000) 2229–2236, https://doi.org/10.1021/ac9913560.
[45] R. Vanna, P. Ronchi, A.T.M. Lenferink, C. Tresoldi, C. Morasso, D. Mehn, M. Bedoni, S. Picciolini, L.W.M.M. Terstappen, F. Ciceri, C. Otto, F. Gramatica, Label-free imaging and identification of typical cells of acute myeloid leukaemia and myelodysplastic syndrome by Raman microspectroscopy, Analyst 140 (2015) 1054–1064, https://doi.org/10.1039/C4AN02127D.
[46] A. Bonifacio, C. Beleites, F. Vittur, E. Marsich, S. Semeraro, S. Paoletti, V. Sergo, Chemical imaging of articular cartilage sections with Raman mapping, employing uni- and multi-variate methods for data analysis, Analyst 135 (2010) 3193–3204, https://doi.org/10.1039/C0AN00459F.
[47] A. Awonusi, M.D. Morris, M.M.J. Tecklenburg, Carbonate assignment and calibration in the raman spectrum of apatite, Calcif. Tissue Int. 81 (2007) 46–52, https://doi.org/10.1007/s00223-007-9034-0.
[48] Y. Liu, L. Tjäderhane, L. Breschi, A. Mazzoni, N. Li, J. Mao, D.H. Pashley, F.R. Tay, Limitations in bonding to dentin and experimental strategies to prevent bond degradation, J. Dent. Res. 90 (2011) 953–968, https://doi.org/10.1177/0022034510391799.
[49] K. Rezwan, Q.Z. Chen, J.J. Blaker, A.R. Boccaccini, Biodegradable and bioactive porous polymer/inorganic composite scaffolds for bone tissue engineering, Biomaterials 27 (2006) 3413–3431, https://doi.org/10.1016/j.biomaterials.2006.01.039.
[50] R. Osorio, E. Osorio, F.S. Aguilera, A.L. Medina-Castillo, M. Toledano, M. Toledano-Osorio, Silver improves collagen structure and stability at demineralized dentin: A dynamic-mechanical and Raman analysis, J. Dent. 79 (2018) 61–67, https://doi.org/10.1016/j.jdent.2018.10.003.
[51] M. Toledano, F.S. Aguilera, E. Osorio, M.T. López-López, I. Cabello, M. Toledano-Osorio, R. Osorio, On modeling and nanoanalysis of caries-affected dentin surfaces restored with Zn-containing amalgam and in vitro oral function, Biointerphases 10 (2015) 041004, https://doi.org/10.1116/1.4933243.
[52] M. Toledano, E. Muñoz-Soto, F.S. Aguilera, E. Osorio, M.P. González-Rodríguez, M. C. Pérez-Álvarez, M. Toledano-Osorio, R. Osorio, A zinc oxide-modified hydroxyapatite-based cement favored sealing ability in endodontically treated teeth, J. Dent. 88 (2019) 103162, https://doi.org/10.1016/j.jdent.2019.06.009.
[53] H. Salehi, E. Terrer, I. Panayotov, B. Levallois, B. Jacquot, H. Tassery, F. Cuisinier, Functional mapping of human sound and carious enamel and dentin with Raman spectroscopy, J. Biophotonics 6 (2013) 765–774, https://doi.org/10.1002/jbio.201200095.
[54] H. Cölfen, Biomineralization: A crystal-clear view, Nat. Mater. 9 (2010) 960–961, https://doi.org/10.1038/nmat2911.
[55] F. Nudelman, K. Pieterse, A. George, P.H.H. Bomans, H. Friedrich, L.J. Brylka, P.A. J. Hilbers, G. de With, N.A.J.M. Sommerdijk, The role of collagen in bone apatite formation in the presence of hydroxyapatite nucleation inhibitors, Nat. Mater. 9 (2010) 1004–1009, https://doi.org/10.1038/nmat2875.
[56] L. Angker, M.V. Swain, Nanoindentation: Application to dental hard tissue investigations, J. Mater. Res. 21 (2006) 1893–1905, https://doi.org/10.1557/jmr.2006.0257.
[57] S. Habelitz, M. Balooch, S.J. Marshall, G. Balooch, G.W. Marshall, In situ atomic force microscopy of partially demineralized human dentin collagen fibrils, J. Struct. Biol. 138 (2002) 227–236, https://doi.org/10.1016/s1047-8477(02)00029-1.
[58] S. Sauro, R. Osorio, T.F. Watson, M. Toledano, Influence of phosphoproteins’ biomimetic analogs on remineralization of mineral-depleted resin-dentin interfaces created with ion-releasing resin-based systems, Dent. Mater. 31 (2015) 759–777, https://doi.org/10.1016/j.dental.2015.03.013.
[59] S. Sauro, R. Osorio, E. Osorio, T.F. Watson, M. Toledano, Novel light-curable materials containing experimental bioactive micro-fillers remineralise mineral-depleted bonded-dentine interfaces, J. Biomater. Sci. Polym. Ed. 24 (2013) 940–956, https://doi.org/10.1080/09205063.2012.727377.
[60] S. Sauro, R. Osorio, T.F. Watson, M. Toledano, Therapeutic effects of novel resin bonding systems containing bioactive glasses on mineral-depleted areas within the bonded-dentine interface, J. Mater. Sci. Mater. Med. 23 (2012) 1521–1532, https://doi.org/10.1007/s10856-012-4606-6.